Atomic structure and glass forming ability of $Cu_{46}Zr_{46}Al_8$ bulk metallic glass

X. D. Wang,[1,a)] Q. K. Jiang,[1] Q. P. Cao,[1] J. Bednarcik,[2] H. Franz,[2] and J. Z. Jiang[1,b)]
[1]*International Center for New-Structured Materials (ICNSM) and Laboratory of New-Structured Materials, Department of Materials Science and Engineering, Zhejiang University, Hangzhou 310027, People's Republic of China*
[2]*HASYLAB am DESY, Notkestrasse 85, D-22603 Hamburg, Germany*

(Received 22 July 2008; accepted 12 September 2008; published online 7 November 2008)

By using a combination of state-of-the-art experimental and computational methods, the high glass forming ability (GFA) of $Cu_{46}Zr_{46}Al_8$ alloy is studied from the view of its atomic packing. Three-dimensional atomic configuration is well established. It is found that Al atoms almost homogeneously distribute around Cu and Zr atoms without segregation, causing the local environment around Cu and Zr atoms in $Cu_{46}Zr_{46}Al_8$ bulk metallic glass different from that of the major competing phase of $Cu_{10}Zr_7$. Furthermore, the addition of Al not only increases the amount of icosahedronlike clusters but also makes them more homogeneous distribution, which can enhance the GFA by increasing the structural incompatibility with the competing crystalline phases. © *2008 American Institute of Physics*. [DOI: 10.1063/1.3009320]

I. INTRODUCTION

Since 1990s, many compositions of bulk metallic glasses (BMGs) with critical size larger than 10 mm in diameter have been discovered in different alloy systems.[1–3] Optimum compositions of glass formers are usually found by trial and error following empirical rules. Moreover, the understanding of the glass forming ability (GFA) is also limited, usually evaluated by some parameters, e.g., the reduced glass transition temperature[4] ($T_{rg}=T_g/T_l$), the extension of the supercooled liquid region[5] ($\Delta T_x=T_x-T_g$), the γ factor[6] ($\gamma=T_x/(T_g+T_l)$) , etc., where T_g is the glass transition temperature, T_l is the liquidus temperature, and T_x is the onset temperature of crystallization. Unfortunately, when using these parameters to evaluate the GFA of BMGs, the contradiction is often encountered, implying that the factors controlling the GFA of BMGs are still undiscovered. However, the GFA is in nature determined by the atomic arrangement and interaction between atoms, i.e., the competition between the amorphous phase and crystalline counterparts upon quenching.

Due to the complicated atomic arrangement in amorphous alloys, it is recognized that the structure of MGs cannot be described by using a single cluster or even by Bernal's polyhedra.[7] Though the cluster model based on face-centered cubic packing can predict compositions of some multicomponent BMGs, the deviation becomes obvious when to fit simple systems such as Ni–B, etc.[8] Recently, the atomic structures of three binary alloys in different systems have been constructed by using their internal "quasiequivalent" clusters.[9] The structure difference between them in the medium range order was clearly demonstrated. Along this line, it becomes possible to understand the structural change in one alloy system with the change in compositions.[10]

Following an empirical rule, at least three components are commonly regarded as a necessary condition for BMG formation. However, for a structure study, a simple system is of great interest. It has been found that BMGs can be produced in the binary Cu–Zr system, for example, $Cu_{50}Zr_{50}$, $Cu_{63.5}Zr_{34.5}$, etc. with critical size up to 2 mm in diameter.[11,12] On addition of Al, the critical size of ternary Cu–Zr–Al BMGs can be above 5 mm.[12,13] The significant increase in critical size of BMGs from binary Cu–Zr to ternary Cu–Zr–Al provides a suitable prototype of BMGs to investigate the structural change behind the increasing GFA by using available experimental and computational methods. In this work, atomic structures of $Cu_{46}Zr_{46}Al_8$ BMG, together with binary $Cu_{50}Zr_{50}$ MG for comparison, have been investigated by a combination of state-of-the-art synchrotron radiation-based [x-ray diffraction (XRD) and extended x-ray absorption fine structure (EXAFS)] and computational [reverse Monte Carlo (RMC)] techniques. The three-dimensional (3D) atomic configuration of the ternary $Cu_{46}Zr_{46}Al_8$ BMG is established. The atomic arrangements from short to medium range order are explored and a favorable configuration is also mapped for $Cu_{46}Zr_{46}Al_8$ BMG with high GFA.

II. EXPERIMENTAL METHODS

Prealloyed ingots of nominal compositions $Cu_{50}Zr_{50}$ and $Cu_{46}Zr_{46}Al_8$ were prepared by arc melting Cu, Zr, and Al with purities higher than 99.9% under a Ti-gettered purified argon atmosphere. From the ingot, a 1 mm thick sheet and a 30 μm thick ribbon were prepared for both alloys by copper mold suction and single roller melt-spinning techniques, respectively. The amorphous nature of the as-cast samples was ascertained by XRD (Philips X'Pert) with Cu $K\alpha$ radiation and differential scanning calorimetry (DSC) (Netzsch DSC 404c). Systematic high quality XRD was measured by using synchrotron radiation with an energy of 100 keV ($\lambda=0.123\ 98$ Å) at the BW5 station, HASYLAB/DESY, Hamburg. Using an image plate detector (Mar345) the two-

a)Author to whom correspondence should be addressed. Electronic mail: wangxd@zju.edu.cn.
b)Electronic mail: jiangjz@zju.edu.cn.

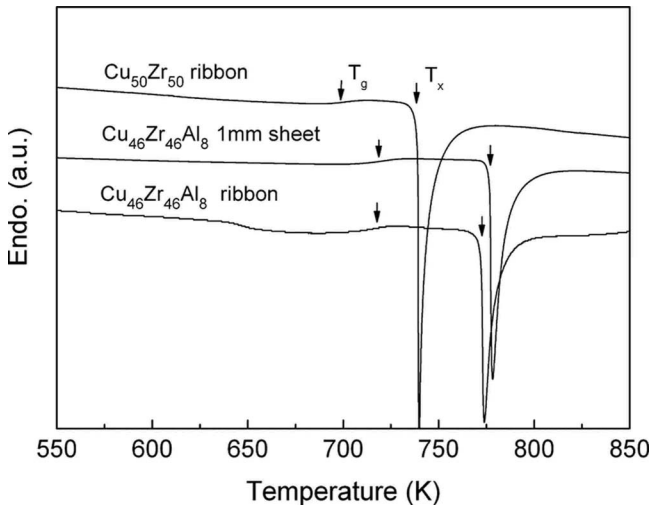

FIG. 1. DSC traces of as-cast $Cu_{50}Zr_{50}$ and $Cu_{46}Zr_{46}Al_8$ MGs at a heating rate of 20 K/min.

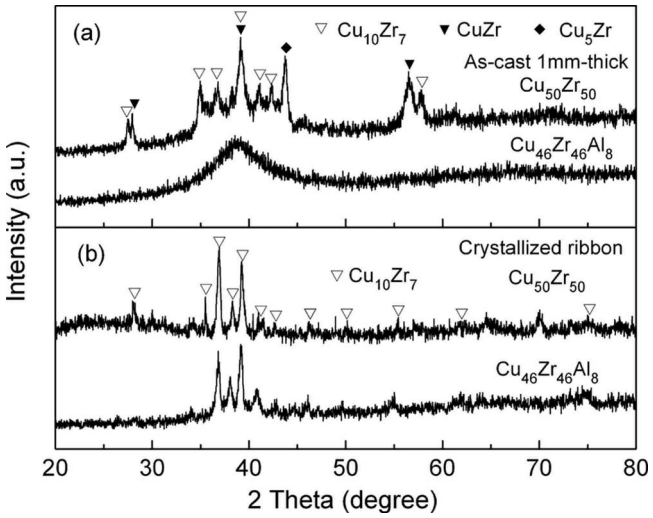

FIG. 2. XRD patterns for (a) 1 mm thick as-cast samples and (b) fully crystallized ribbon samples of $Cu_{50}Zr_{50}$ and $Cu_{46}Zr_{46}Al_8$ MGs.

dimensional intensity distribution was collected up to a large wave-vector transfer. The radially averaged scattering intensity $I(q)$ ($q=4\pi \sin \theta/\lambda$) was extracted by using the software package FIT2D.[14] From $I(q)$, the structure factor $S(q)$ and the pair distribution function (PDF) $G(r)$ could be obtained by using PDFGETX2.[15] EXAFS spectra at the Cu K-edge (8979 eV) and the Zr K-edge (17 998 eV) were collected in transmission mode at the beamline $X1$ at HASYLAB. Standard data analysis was carried out by the program package VIPER.[16]

III. RESULTS

A. Difference in glass forming ability

Figure 1 shows the DSC curves of as-cast $Cu_{50}Zr_{50}$ and $Cu_{46}Zr_{46}Al_8$ MGs at a heating rate of 20 K/min. It is seen that the samples of $Cu_{46}Zr_{46}Al_8$ MG in the shape of 30 μm thick ribbon and 1 mm thick sheet basically exhibit the same glass transition temperature T_g and crystallization onset temperature T_x, which are obviously higher than those for $Cu_{50}Zr_{50}$ MG, indicating that the ternary $Cu_{46}Zr_{46}Al_8$ MG is more stable than the binary $Cu_{50}Zr_{50}$ MG. Figure 2(a) shows the XRD patterns of as-cast $Cu_{50}Zr_{50}$ and $Cu_{46}Zr_{46}Al_8$ MGs measured on the 1 mm thick sheets. Sharp peaks corresponding to Bragg diffraction of crystalline phases are clearly observed in the $Cu_{50}Zr_{50}$ alloy. The phases are identified, mainly $Cu_{10}Zr_7$ phase with minor share of CuZr and Cu_5Zr. However, only a broad diffraction maximum is detected for the $Cu_{46}Zr_{46}Al_8$ alloy, indicating its fully amorphous nature. As such, it is clear that the addition of Al significantly promotes the GFA of the ternary $Cu_{46}Zr_{46}Al_8$ alloy. To compare the phase formation in both MGs, the ribbon samples were heated by DSC to the temperature where the crystallization events just initiated, and also to the temperature the events were complete, then cooled down to ambient temperature. Unlike rapid quenching, the phase that precipitated in both MGs is $Cu_{10}Zr_7$, as shown in the XRD patterns displayed in Fig. 2(b). We conclude that the phase $Cu_{10}Zr_7$, as the major competing phase, can be more easily precipitated upon cooling and heating in $Cu_{50}Zr_{50}$ alloy than in $Cu_{46}Zr_{46}Al_8$ alloy. In other words, the addition of Al changes the atomic arrangement of Cu and Zr atoms and suppresses the formation of the orthorhombic $Cu_{10}Zr_7$ phase in $Cu_{46}Zr_{46}Al_8$.

B. Structure difference by synchrotron radiation x-ray diffraction

The effective atomic arrangement is determined by the interaction between atoms that can be described by an effective size attributed to each element. In the Cu–Zr–Al system, the Goldschmidt atomic radii of components are 1.28 Å for Cu, 1.6 Å for Zr, and 1.43 Å for Al. The heat of mixing of Cu–Zr, Cu–Al, and Zr–Al is −23 kJ/mol, −1 kJ/mol, and −44 kJ/mol,[17] respectively. Thus, the addition of Al, due to the intermediate atomic size and strong interaction with Cu and Zr atoms, can increase the packing density and suppress the movement of atoms. By using high energy synchrotron radiation x-ray, we measured the diffraction data up to high q values (16 $Å^{-1}$) and transformed them into the PDFs $G(r)$ for two MGs, as shown in Fig. 3. The $G(r)$ curves of both MGs are quite analogous. However, $Cu_{46}Zr_{46}Al_8$ in bulk (1 mm sheet) shows slightly higher local ordering since the

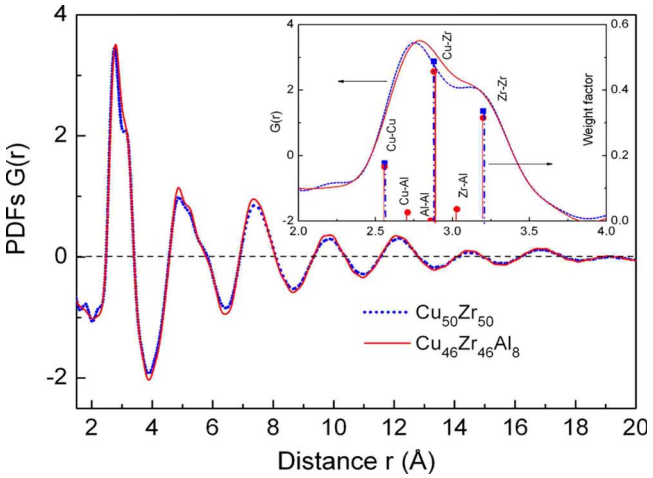

FIG. 3. (Color online) PDF $G(r)$ for $Cu_{50}Zr_{50}$ and $Cu_{46}Zr_{46}Al_8$ MGs. The inset is the local magnification of the first peak in $G(r)$ of two MGs with the weight factors w_{ij} of atomic pairs in the nearest neighbor shell.

amplitude in $G(r)$ is a little higher compared with the $Cu_{50}Zr_{50}$ alloy (ribbon) on several neighbor shells. Also, from the inset in the figure showing the local magnification of the first peak in $G(r)$, one can find that the shoulder between Cu–Zr and Zr–Zr pairs becomes smeared out in $Cu_{46}Zr_{46}Al_8$ when compared with $Cu_{50}Zr_{50}$. The weight factors reflect the contribution of partial atomic pairs to the total PDF, which can be calculated from the atomic form factor $f(q)$ by using the following equation:[18]

$$w_{ij} = \frac{(2-\delta_{ij})c_i c_j f_i(q) f_j(q)}{\sum_{ij} c_i c_j f_i(q) f_j(q)},$$

where c is the concentration of each component and δ_{ij} is the Kronecker delta. The value of weight factors and the lengths of different pairs (evaluated by the model of hard spheres) are also listed in the inset of Fig. 3, showing that the intermediate positions are filled with Cu–Al, Al–Al, and Zr–Al atomic pairs.

C. Structure simulation by RMC

In order to get a more reliable atomic structural configuration, we performed RMC simulations by using three experimental data set *simultaneously* [one $S(q)$ and two EXAFS spectra]. The simulation box contained 10 000 atoms. The length of the box used was 54.983 Å for $Cu_{50}Zr_{50}$ MG and 54.970 Å for $Cu_{46}Zr_{46}Al_8$ BMG according to their atomic densities. The cutoff distances of Cu–Cu (2.3 Å), Cu–Zr (2.45 Å), Zr–Zr (2.8 Å), Cu–Al (2.35 Å), Zr–Al (2.5 Å), and Al–Al (2.4 Å) were adopted throughout the simulation runs. Figures 4(a) and 4(b) display the comparison in $S(q)$ and EAXFS spectra (Cu and Zr K-edge) between experimental data (solid line) and simulated ones (dotted line) for $Cu_{46}Zr_{46}Al_8$ BMG, showing good agreements between them. Similar fitting results were obtained for $Cu_{50}Zr_{50}$ MG (not shown here). The 3D atomic structure for both MGs resulting from the fitting procedure is shown in Fig. 4(c).

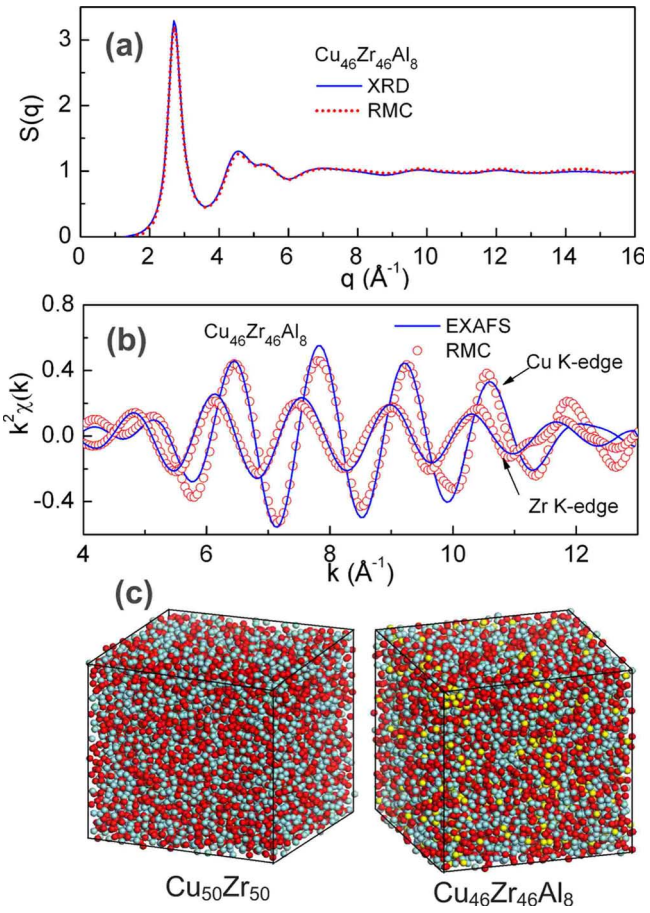

FIG. 4. (Color online) (a) and (b) Comparison in $S(q)$ and EXAFS spectra of experimental data (solid line) with RMC simulated data (dotted line) for $Cu_{46}Zr_{46}Al_8$ BMG, respectively. (c) 3D atomic configurations (red: Cu, gray: Zr, and yellow: Al) for $Cu_{50}Zr_{50}$ MG and $Cu_{46}Zr_{46}Al_8$ BMG.

IV. DISCUSSION

A. Voronoi tessellation analysis

To further deduce the local structure of clusters, the Voronoi method was employed setting a cutoff distance of 3.5 Å.[19] Total fractions of various clusters centered by Cu, Zr, and Al atoms with different coordination numbers (CNs) in these two MGs are shown in Fig. 5(a) while clusters with their fractions less than 1% are not considered. It is clear that icosahedronlike clusters with CN=12 are dominant in both MGs. However, polyhedra with CN=12 and 13 are found in larger amounts in $Cu_{46}Zr_{46}Al_8$ than in $Cu_{50}Zr_{50}$ MG. Others with CN=(9,10,11) and (14,15) are less.

The average number of nearest neighbors around Cu atoms is of about 11.5 and about 12.8 around Zr atoms, leading to the totally average CN of 12.1 for $Cu_{50}Zr_{50}$ MG. Accordingly, the total value of the CN for $Cu_{46}Zr_{46}Al_8$ is of about 12.2 and partial coordination values of about 11.8 around Cu atoms, 12.6 around Zr atoms, and 11.4 around Al atoms. In details, Fig. 5(b) demonstrates the distribution of polyhedra with different coordinates centered by atoms of each component for both MGs. The polyhedra with CN=11 around Cu atoms and CN=13 around Zr atoms constitute the majority in $Cu_{50}Zr_{50}$ MG. On addition of Al, the amount of 10 and 11-coordinated polyhedra centered by Cu atoms greatly decreased, while the polyhedra with high CN, such as 12, 13, and 14-coordinated, become favorable in $Cu_{46}Zr_{46}Al_8$ BMG. However, the variation in polyhedra around Zr atoms is just vice versa. It is obvious that Al addition makes the distribution of polyhedra centered by Cu and Zr atoms more concentrated, approaching 12 and 13-coordinated structures in $Cu_{46}Zr_{46}Al_8$ BMG. Interestingly, when checking the distribution of Al atoms in the nearest neighbor shell of Cu and Zr atoms, it is found that the distribution of Al is almost half-and-half, as demonstrated in Fig. 5(c), rather than having a stronger segregation to Zr atoms at present concentration, although the affinity between Zr and Al is much stronger than between Cu and Al.

The dominant polyhedron with CN=11 is $\langle 0,2,8,1\rangle$, which amounts to 9.13% in $Cu_{50}Zr_{50}$ and 7.72% in $Cu_{46}Zr_{46}Al_8$. In both MGs, the amount of the ideal icosahedron of $\langle 0,0,12,0\rangle$ is rather low. Most of polyhedra with CN=12 are icosahedronlike or distorted icosahedra with index of $\langle 0,2,8,2\rangle$ and $\langle 0,3,6,3\rangle$. From atomic configurations obtained from RMC, the quasiequivalent clusters are deduced and packed to fill the 3D space in these two MGs by

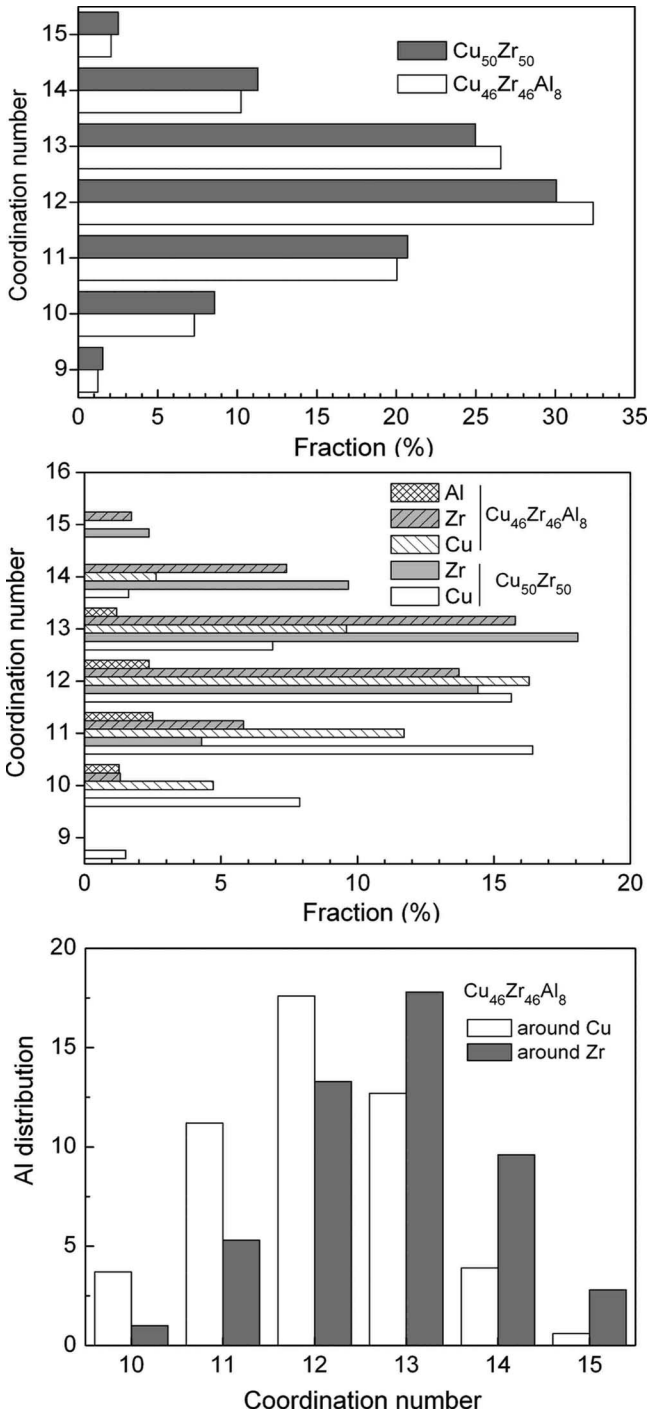

FIG. 5. (a) Total fraction of each kind of polyhedron and (b) fraction of polyhedra centered by Cu, Zr, and Al atoms with different CNs in $Cu_{50}Zr_{50}$ MG and $Cu_{46}Zr_{46}Al_8$ BMG, respectively. (c) Distribution of Al atoms on the polyhedra around Cu and Zr atoms in $Cu_{46}Zr_{46}Al_8$ BMG.

face, edge, and vertex sharing. It is found that the medium range order is changing from atom to atom. However, the

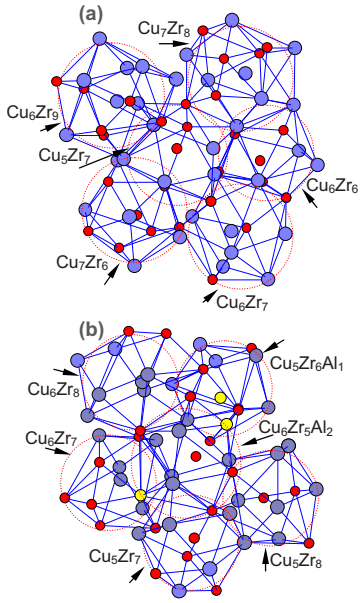

FIG. 6. (Color online) Packing of quasiequivalent clusters showing the medium-range order in (a) $Cu_{50}Zr_{50}$ MG and (b) $Cu_{46}Zr_{46}Al_8$ BMG.

medium range atomic packing, i.e., icosahedra companying with 11 and 14-coordinated polyhedra such as Cu_6Zr_6, Cu_5Zr_7, Cu_7Zr_8, Cu_6Zr_9, etc., is often found in $Cu_{50}Zr_{50}$ MG, while in $Cu_{46}Zr_{46}Al_8$ BMG the atomic packing, more icosahedral clusters companying with 12-coordinated polyhedra such as Cu_6Zr_7, $Cu_6Zr_5Al_2$, etc., is detected with high probability, as illustrated in Figs. 6(a) and 6(b).

B. Local structure in Cu_5Zr and $Cu_{10}Zr_7$ phases

Upon uniaxial compression of $Cu_{50}Zr_{50}$ BMG, the phase of Cu_5Zr was detected in the shear bands by high resolution transmission electron microscopy (HRTEM),[20] suggesting that it may be the primary or metastable phase induced by deformation. The space group of this phase is F_{43m} (No. 216) with lattice parameter of $a=6.87$ Å. Using the cutoff of $r=3.5$ Å, the outside environment of its three nonequivalent atoms, one Zr and two Cu, is 16 Cu atoms, 9 Cu plus 3 Zr atoms, and 12 Cu plus 4 Zr atoms, respectively. In addition, the phase $Cu_{10}Zr_7$, as a major competing phase upon the glass formation, has the space group Aba_2 (No. 41) and lattice parameters $a=9.3467$ Å, $b=9.3163$ Å, and $c=12.6729$ Å.[21] In this phase, there are ten nonequivalent sites of five Zr atoms and five Cu atoms. By checking the nearest neighbor environment of these ten nonequivalent atoms within $r=3.5$ Å, the different atomic configurations of the nearest neighbor are obtained and listed in Table I. It is confirmed that the CNs are of 10 and 11 around Cu atoms and 12, 14, and 16 around Zr atoms. Comparing with the

TABLE I. CNs and the type of atoms in the nearest neighbor around ten nonequivalent sites of the $Cu_{10}Zr_7$ phase.

Sites	Zr_1	Zr_2	Zr_3	Zr_4	Zr_5	Cu_1	Cu_2	Cu_3	Cu_4	Cu_5
CN	12	16	16	14	16	10	11	11	11	10
Atoms	Cu_8Zr_4	$Cu_{10}Zr_6$	$Cu_{10}Zr_6$	Cu_8Zr_6	$Cu_{10}Zr_6$	Cu_5Zr_5	Cu_4Zr_7	Cu_4Zr_7	Cu_4Zr_7	Cu_4Zr_6

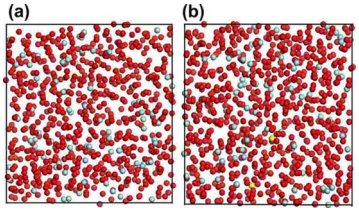

FIG. 7. (Color online) Distribution of icosahedronlike clusters in (a) $Cu_{50}Zr_{50}$ and (b) $Cu_{46}Zr_{46}Al_8$ MGs represented by the position of their central atoms viewed along an edge of simulation box.

distribution in CN centered by atoms of different elements for both MGs in Fig. 5(b), it is found that the local structure in $Cu_{10}Zr_7$ phase is much closer to the atomic configuration of $Cu_{50}Zr_{50}$ MG. This might indirectly explain why $Cu_{10}Zr_7$ phase easily precipitates in $Cu_{50}Zr_{50}$ MG. In addition, by performing Rietveld refinement of the XRD patterns in Fig. 2, the lattice parameters obtained are $a=9.4127$ Å, $b=9.2879$ Å, and $c=12.7360$ Å for $Cu_{10}Zr_7$ phase in $Cu_{50}Zr_{50}$ MG and $a=9.4586$ Å, $b=9.3277$ Å, and $c=12.7988$ Å for $Cu_{10}Zr_7$ phase in $Cu_{46}Zr_{46}Al_8$ BMG, respectively. The increase in lattice parameters for the $Cu_{10}Zr_7$ phase in $Cu_{46}Zr_{46}Al_8$ BMG indicates that Al atoms preferably replace Cu atoms, which most likely hinders the movement of Cu and Zr atoms during crystallization to form proper short range order, leading to the high stability of this BMG accordingly. A similar conclusion was also reported for the effect of Al in Zr–Cu-based alloys.[22]

C. Distribution of icosahedra

The icosahedron was first proposed as a structure unit for liquids.[23] Later it was experimentally confirmed that it exists in liquids,[24] amorphous alloys,[25] and quasicrystals as well, and plays important roles in the properties of these materials. In the Cu–Zr alloy system, fivefold icosahedral or icosahedronlike clusters are found to be dominant over a wide composition range, which increase the structural incompatibility with the competing crystalline phases, resulting in the high GFA of this alloy system.[10,26] As mentioned above, the amounts of 12-coordinated clusters are dominant in both MGs, amounting to 30.1% in $Cu_{50}Zr_{50}$ and 32.4% in $Cu_{46}Zr_{46}Al_8$. The distribution of icosahedronlike clusters in both MGs is further examined by checking the position of central atoms. Only those icosahedronlike clusters are considered that show face, edge, and vertex sharing. It is found that the distribution of these clusters is more homogeneous in $Cu_{46}Zr_{46}Al_8$ BMG than in $Cu_{50}Zr_{50}$ MG where they are more inclined to segregate together, as shown in Fig. 7, along an edge of the simulation box. Thus, other polyhedra could be separated by icosahedronlike clusters in $Cu_{46}Zr_{46}Al_8$ BMG. This possibly increases the energy barrier in forming crystalline phases, contributing also to the high stability and GFA of $Cu_{46}Zr_{46}Al_8$ BMG.

V. CONCLUSIONS

Atomic structures of BMG-forming $Cu_{46}Zr_{46}Al_8$ together with the binary $Cu_{50}Zr_{50}$ metallic glasses have been studied by a combination of state-of-the-art experimental and computational techniques. By elucidating the structure difference in 3D atomic configuration between two MGs, we attempted to explain high GFA of ternary $Cu_{46}Zr_{46}Al_8$ alloy from three aspects of atomic structure: (1) rather homogeneous distribution of Al atoms around Cu and Zr atoms, (2) modifying the environment around Cu and Zr atoms away from the local structure of the competing crystalline phase, and (3) increasing the amount of icosahedronlike clusters and making their distribution more homogeneous among different polyhedra in 3D space. We believe that the results obtained here will trigger more atomic structure studies to uncover the nature of the GFA for various systems.

ACKNOWLEDGMENTS

The authors would like to thank the HASYLAB staff at Hamburg, Germany for the assistance during the measurements at BW5 and X1. Financial support from the National Natural Science Foundation of China (Grant Nos. 50425102, 50601021, 50701038, and 60776014), Zhejiang University-Helmholtz cooperation fund, the Ministry of Education of China (Program for Changjiang Scholars and the Research Fund for the Doctoral Program of Higher Education), and Zhejiang University are gratefully acknowledged.

[1] A. L. Greer, Science **267**, 1947 (1995).
[2] W. L. Johnson, MRS Bull. **24**, 42 (1999).
[3] A. Inoue, Acta Mater. **48**, 279 (2000).
[4] D. Turnbull, Contemp. Phys. **10**, 473 (1969).
[5] T. Zhang, A. Inoue, and T. Masumoto, Mater. Trans., JIM **32**, 1005 (1991).
[6] Z. P. Lu and C. T. Liu, Acta Mater. **50**, 3501 (2002).
[7] J. D. Bernal, Nature (London) **185**, 68 (1960).
[8] D. B. Miracle, Nature Mater. **3**, 697 (2004).
[9] H. W. Sheng, W. K. Luo, F. M. Alamgir, J. M. Bai, and E. Ma, Nature (London) **439**, 419 (2006).
[10] X. D. Wang, S. Yin, Q. P. Cao, J. Z. Jiang, H. Franz, and Z. H. Jin, Appl. Phys. Lett. **92**, 011902 (2008).
[11] D. Wang, Y. Li, B. B. Sun, M. L. Sui, K. Lu, and E. Ma, Appl. Phys. Lett. **84**, 4029 (2004).
[12] P. Yu, H. Y. Bai, M. B. Tang, and W. L. Wang, J. Non-Cryst. Solids **351**, 1328 (2005).
[13] D. Wang, H. Tan, and Y. Li, Acta Mater. **53**, 2969 (2005).
[14] A. P. Hammersley, S. O. Svensson, M. Hanfland, A. N. Fitch, and D. Häusermann, High Press. Res. **14**, 235 (1996).
[15] I.-K. Jeong, J. Thompson, A. M. P. Turner, and S. J. L. Billinge, J. Appl. Crystallogr. **34**, 536 (2001).
[16] K. V. Klementev, J. Phys. D **34**, 209 (2001).
[17] F. R. Boerde, R. Boom, W. C. M. Matterns, A. R. Miedema, and A. K. Niessen, *Cohesion in Metals* (North-Holland, Amsterdam, 1998).
[18] K. Saksl, P. Jovari, H. Franz, Q. S. Zeng, J. F. Liu, and J. Z. Jiang, J. Phys.: Condens. Matter **18**, 7579 (2006).
[19] J. L. Finney, Proc. R. Soc. London, Ser. A **319**, 479 (1970).
[20] M. W. Chen, A. Inoue, W. Zhang, and T. Sakurai, Phys. Rev. Lett. **96**, 245502 (2006).
[21] L. Bsenko, J. Less-Common Met. **40**, 365 (1975); M. E. Kirkpatrick, J. F. Smith, and W. L. Larsen, Acta Crystallogr. **15**, 894 (1962).
[22] L. Q. Xing, P. Ochin, and J. Bigot, J. Non-Cryst. Solids **205–207**, 637 (1996).
[23] F. C. Frank, Proc. R. Soc. London, Ser. A **215**, 43 (1952).
[24] H. Reichert, O. Klein, H. Dosch, M. Denk, V. Honkimäki, T. Lippmann, and G. Reiter, Nature (London) **408**, 839 (2000).
[25] K. Saksl, H. Franz, P. Jóvári, K. Klementiev, E. Welter, A. Ehnes, J. Saida, A. Inoue, and J. Z. Jiang, Appl. Phys. Lett. **83**, 3924 (2003); W. K. Luo, H. W. Sheng, F. M. Alamgir, J. M. Bai, J. H. He, and E. Ma, Phys. Rev. Lett. **92**, 145502 (2004).
[26] L. Yang, J. H. Xia, Q. Wang, C. Dong, L. Y. Chen, X. Ou, J. F. Liu, J. Z. Jiang, K. Klementiev, K. Saksl, H. Franz, J. R. Schneider, and L. Gerward, Appl. Phys. Lett. **88**, 2419131 (2006).